

### ITU/MMEJ

# Enhanced Tribological Performance of Micro-Arc Oxidation Coatings on 7075 Aluminium Alloy via Zn-Enriched Cold Spray Layers

Gizem Kullu , Mertcan Kaba , Faiz Muhaffel , Huseyin Cimenoglu

Metallurgical and Materials Engineering Department, Istanbul Technical University, Maslak 34469 Istanbul – Türkiye.

Keywords: Aluminium, micro arc oxidation, cold spray, wear resistance, lubrication.

# 7075 Alüminyum Alaşımı Yüzeyinde Zn İçeren Soğuk Püskürtme Tabakası Üzerinde Oluşturulan Mikro Ark Oksidasyon Kaplamaların Tribolojik Performansının İyileştirilmesi

Özet: Alüminyum alaşımları, yüksek mukavemet/ağırlık oranları ve korozyon dirençleri nedeniyle çeşitli endüstrilerde yaygın olarak kullanılmaktadır; ancak düşük aşınma dirençleri, zorlu koşullarda kullanımlarını sınırlandırmaktadır. Yüzey modifikasyon işlemleri, bu alaşımların aşınma davranışını iyileştirerek uygulama alanlarını genişletebilme potansiyeline sahiptir. Bu çalışmada, 7075 alüminyum alaşımı üzerine soğuk püskürtme (CS) yöntemiyle biriktirilen Al-Zn tabakalar üzerinde oluşturulan mikro-ark oksidasyon (MAO) kaplamalarının mikroyapısal özellikleri ve tribolojik davranışları incelenmiştir. Bu çalışmada, CS tabakasındaki Zn miktarının (ağırlıkça %0'dan %60'a kadar) üretilen MAO kaplamalarının özellikleri üzerindeki etkisi araştırılmıştır. Kaplamaların karakterizasyonu X-ışını kırınımı (XRD), taramalı elektron mikroskobu (SEM) ve Al<sub>2</sub>O<sub>3</sub> bilya ile gerçekleştirilen kuru kayma aşınma testleri kullanılarak yapılmıştır. MAO kaplamaları, ortalama olarak yaklaşık 25 μm kalınlığa sahiptir ancak %60 Zn içeren CS tabakasındaki MAO kaplama tabakası yaklaşık 15 μm kalınlığa düşmüştür. MAO uygulanmış Al-Zn kaplamaları, ağırlıklı olarak α-Al<sub>2</sub>O<sub>3</sub> ve γ-Al<sub>2</sub>O<sub>3</sub> fazları ile birlikte ZnO'dan oluşmuştur. Aşınma testleri sonuçları, en düşük sürtünme katsayısının (COF = 0,18; 1 N yük altında) ve en yüksek aşınma direncinin, %30 Zn içeren CS tabakası üzerine uygulanan MAO kaplamasında elde edilememiştir. Sonuç olarak, bu çalışmanın ön bulguları değerlendirildiği zaman, düşük sürtünme katsayısı ve yüksek aşınma direncinin gerekli olduğu endüstriyel uygulamalarda CS ve MAO kaplama proseslerinin alüminyum alaşımlarının kullanımını genişletme potansiyeline sahip olduğu düşünülmektedir.

Anahtar Kelimeler: Alüminyum, mikro ark oksidasyon, soğuk püskürtme, aşınma direnci, yağlama.

#### Article

Corresponding Author: Huseyin Cimenoglu, E-mail: cimenogluh@itu.edu.tr

Reference: Kullu, G., Kaba, M., Muhaffel, F. and Cimenoglu, H., (2025), Enhanced Tribological Performance of Micro-Arc Oxidation Coatings on 7075 Aluminium Alloy via Zn-Enriched Cold Spray Layers, ITU Journal of Metallurgy and Materials Engineering, 1(2) 29–35.

Submission Date : 8 March 2025 Online Acceptance : 18 April 2025 Online Publishing : 22 April 2025



#### 1. Introduction

Aluminium (AI) and its alloys have drawn interest in a broad range of application areas thanks to their high specific strength, excellent formability, and ease of fabrication. Also, they reduce CO<sub>2</sub> emissions by lowering vehicle weight due to their low density and high specific strength. Considering these essential advantages, aluminium alloys have become very attractive materials for the aerospace and automotive industries (Prasad & Wanhill, 2016). Among the AI alloys, the 7XXX series, which have zinc (Zn) as the primary alloying element, are favoured for applications requiring high strength (Gándara, 2013). Specifically, 7075 AI alloy is very common and widely used in aerospace applications due to its excellent strength-to-weight ratio.

Although 7075 Al alloy has several advantages, it does not exhibit sufficient tribological properties because of its unstable and high friction coefficient, low hardness and wear resistance. Different surface modification techniques have been developed in order to overcome these limitations. In this regard, thick and adherent oxide forming micro-arc oxidation (MAO), also referred to as plasma electrolytic oxidation (PEO), has received considerable attention, as it offers numerous advantages, including excellent protection of the substrate from wear and corrosion (Jiang & Wang, 2010). In the open literature, many attempts have been made to enhance the wear properties of 7075 Al alloy with MAO coating (Lv, Cao, Wan, & Xu, 2019; Muhaffel, Baydogan, & Cimenoglu, 2021; Rama Krishna, Somaraju, & Sundararajan, 2003; Yang, Chen, Jin, Du, & Xue, 2019).

On the other hand, considering the possible adverse effects of micro-cracks and micro-pores present in the structure of MAO coatings (Curran & Clyne, 2006). Some attempts, like introducing particles into the MAO coating, have been made by employing the MAO process in various particle-added electrolytes (Lu et al., 2016). For example, remarkable enhancement in hardness and wear resistance has been detected by Muhaffel et al. (Muhaffel et al., 2021) from the zirconia (ZrO<sub>2</sub>) and alumina (Al<sub>2</sub>O<sub>3</sub>) incorporated MAO coatings fabricated on 7075 Al alloy. On the other hand, upon the incorporation of solid lubricant particles (such as graphite and MoS<sub>2</sub>) into the MAO coating, the friction coefficient is reduced, and tribological properties are improved.

As a novel approach, Tazegül et al. (Tazegul et al., 2014) produced a multi-layered alumina coating on AZ91D Mg alloy by combining cold spray (CS) and MAO processes. They first deposited the Al layer on the AZ91D alloy by CS. Then, MAO was synthesised to form an external alumina coating. It is finally concluded that multilayer coating produced by the combination of CS and MAO processes is very promising for the protection of Mg alloys against corrosion and wear at room temperature (RT). Recently, Kaba et al. (Kaba, Muhaffel, Malayoglu, & Cimenoglu, 2024) detected the success of this type of multilayer coating in the protection of WE43 Mg alloy against high-temperature dry sliding wear up to 350 °C.

Based on the attractive properties of multilayer coatings for protecting Mg alloys against wear under dry sliding contact, this study was initiated to extend combining CS and MAO processes to Al alloys. Considering the HCP structure-related lubricity effect of Zn, prior to the MAO process, various amounts of Zn powder containing (up to 60 wt.%) Al powder mixtures were deposited on 7075 alloy by CS process. Then, these samples were subjected to dry sliding wear tests at RT against an Al<sub>2</sub>O<sub>3</sub> ball to reveal their tribological performances.

# 2. Materials and Methods2.1 CS process

In the present study, the CS process was applied to 7075 Al alloy disc samples having a diameter of 16 mm and thickness of 4 mm. Before the CS process, samples were ground by SiC abrasive paper with a grit size of P320, then cleaned with ethanol, and later dried in air at RT. Al (7–15  $\mu$ m, 99.5% purity) and Zn (6–9  $\mu$ m, 97.5% purity) powders, both supplied by Alfa

Aesar, were used as feedstock materials in the CS process. CS was carried out on 7075 Al substrate samples by using particle mixing of Al-Zn with the wt.% ratios of 85:15, 70:30, and 40:60. CS process was employed with RUSONIC Model K-201 low-pressure CS equipment having converging-diverging-type tubular nozzle with an expansion ratio of 2:3. During CS process, six bar inlet pressure of air was used. Also, transverse speed was determined as 1 mm/s for every deposition. Furthermore, the stand-off distance and distance between passes were applied to 10 mm and 2 mm, respectively.

#### 2.2 MAO process

Before the MAO process, CS'ed samples were ground by SiC abrasive papers up to a grit size of P2500, then cleaned with ethanol, and finally dried in air at RT. For the MAO process, a 30-kW bipolar pulsed DC power supply unit, a stainless-steel electrolyte bath, an air pump for stirring the electrolyte solution, and an external cooling system were used. During the process, the sample was connected to the electrochemical cell as the anode, while the stainless-steel container acted as the cathode.

MAO process was conducted in an electrolyte solution consisting of 10 g/L NaAlO2 (Alfa Aesar), 2 g/L Na3PO4 (Alfa Aesar), and 2 g/L KOH (Alfa Aesar) with distilled water. The MAO coatings were produced on CS'ed samples by using a constant voltage of 520 V in the positive half cycle and 80 V in the negative half cycle. The pulse frequency, positive and negative voltage pulse ratio and duty cycle were 500 Hz, 1:1 and 40%, respectively. 7075 Al alloy samples were treated for 5 min during the MAO process. Finally, samples were subjected to ultrasonic cleaning with ethanol and distilled water and later dried in the air at RT. Electrolyte temperature was kept below 25 °C via the external cooling system in order to prevent evaporation of electrolyte solution and adjust the chemical reaction rate in the interface of electrolyte/sample.

Hereafter, MAO coatings on CS'ed samples will be referred to as CS-MAO-15Zn, CS-MAO-30Zn, and CS-MAO-60Zn. Apart from the MAO coatings fabricated on CS'ed samples, 7075 Al alloy disc samples were subjected to only the MAO process without CS by using the same electrolyte composition. This sample will be referred to as MAO.

#### 2.3. Microstructural characterisation

An X-ray diffractometer (XRD, GBC MMA 028) was used by using Cu-K $\alpha$  radiation in order to determine the phase composition of the coatings. For this purpose, XRD analysis was performed at 2 $\theta$  range between 20-80 $^{\circ}$  at a step of 0.020 $^{\circ}$  and a scanning speed of 1 $^{\circ}$ /min.

Surface morphology and cross-section of the samples were examined by scanning electron microscope (SEM, Hitachi TM-1000 and FEI XL30 SFEG) in order to determine the microstructure of the coatings. An energy-dispersive X-ray spectrometer (EDX) was also used to assess the wt.% of the elements in the coatings. The mean surface roughness (Ra) value of the coatings was measured by a 2-D contact surface profilometer (Veeco Dektak 6M).



#### 2.4. Wear Tests

Before the wear tests, the samples were ground with SiC paper with a grit size of P2500 to reduce surface asperities. The wear tests were performed on the samples with a ball-on-disc tribometer (Tribotech) at RT using a counterface as an  $Al_2O_3$  ball 6 mm in diameter. The counterface followed a reciprocating path of 5 mm on the sample surface at a sliding speed of 10 mm/s. Wear tests were carried out at loads of 1, 2, 3, and 4 N for a total sliding distance of 50 m. The friction curves were recorded during the wear tests by the software of the wear test device. Following the wear tests, worn surfaces were examined by SEM. Specific wear rates of the samples were calculated by measuring 2-D profiles of the wear tracks.

# 3. Results and Discussion3.1 Structural features

The XRD spectra of MAO and CS-MAO-Zn samples with varying Al-Zn compositions are presented in Figure 1. The MAO sample exhibited Al $_2O_3$  phases in both  $\alpha\text{-}$  and  $\gamma\text{-}$  forms. Additionally, the presence of the MgZn $_2$  peak from the substrate was detected due to the penetration of X-rays beyond the coating. Similarly, CS-MAO-Zn samples contained Al and Al $_2O_3$  phases, while Zn-related phases, including Zn and ZnO, were introduced into the coating through Zn addition during the CS process. XRD results confirmed the successful integration of Zn particles into the coating via the CS process. Phases of Na, K, and P elements present in the electrolyte were not detected in XRD analysis.

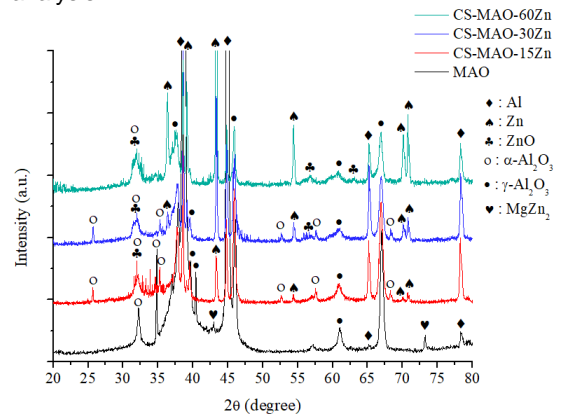


Figure 1. XRD spectra of MAO and CS-MAO-Zn samples with varying Al:Zn compositions.

Şekil 1. Farklı Al:Zn bileşimlerine sahip MAO ve CS-MAO-Zn numunelerinin XRD spektrumları.

Figure 2 presents the surface and cross-sectional SEM images of MAO and CS-MAO-Zn samples with different Al:Zn compositions. Surface SEM images revealed that both MAO and CS-MAO-Zn samples exhibited characteristic pancake structures with micropores formed due to spark discharge phenomena related to the MAO process. Furthermore, the CS-MAO-30Zn sample had smaller surface pores than the others. Surface roughness measurements indicated that CS-MAO-30Zn had the lowest surface roughness at 0.84 ± 0.12 µm, whereas the MAO sample exhibited the highest roughness at 1.56 ± 0.16 µm. Cross-sectional SEM images showed distinct CS and MAO layers, with lower porosity in the MAO, CS-MAO-15Zn, and CS-MAO-30Zn samples, while the CS-MAO-60Zn sample displayed a more porous structure. Additionally, ZnO particles were distinctly observed in the CS-MAO-30Zn sample, appearing as bright regions highlighted in red circles.

Among the CS'ed samples, the CS-MAO-60Zn sample exhibited the highest porosity (both in the CS layer and MAO coating) while the CS-MAO-30Zn sample displayed smaller, more uniform pores on their cross-sections, with the CS layers having at least 100  $\mu m$  in thickness before the MAO process.

SEM examinations further revealed that the MAO layer thickness was approximately 25  $\mu m$  for the MAO, CS-MAO-15Zn, and CS-MAO-30Zn samples, maintaining a uniform thickness, whereas the CS-MAO-60Zn coating had a less homogeneous structure with a reduced thickness of around 15  $\mu m$ . EDX analysis of the CS layers showed that the CS-MAO-30Zn and CS-MAO-60Zn samples contained 34.37 wt.% and 75.56 wt.% Zn, respectively, confirming that Zn particle integration closely matched the theoretical values after the CS process.

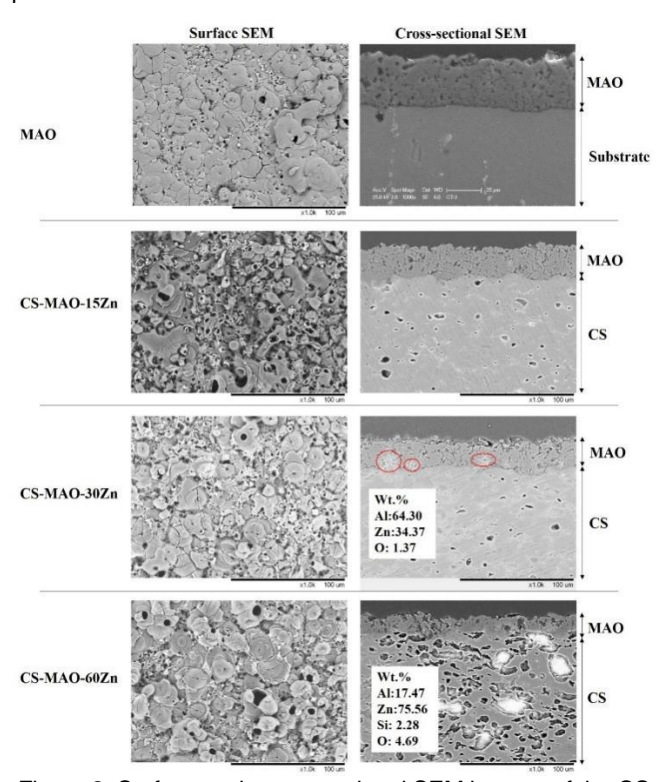


Figure 2. Surface and cross-sectional SEM images of the CS-MAO-Zn samples with varying Al:Zn compositions. Şekil 2. Farklı Al:Zn bileşimlerine sahip CS-MAO-Zn numunelerinin yüzey ve kesit SEM görüntüleri.

Figure 3 presents the elemental mapping analysis of the cross-section of the CS-MAO-30Zn sample. The results confirmed the presence of Al and Zn in both the MAO and CS layers. As a result of the oxide phases formed during the MAO process, the MAO coating was distinguished from the CS layer underneath with a high concentration of O. Additionally, Zn/ZnO phases were detected beneath the oxide MAO layer, further verifying the successful integration of Zn particles during the CS process.

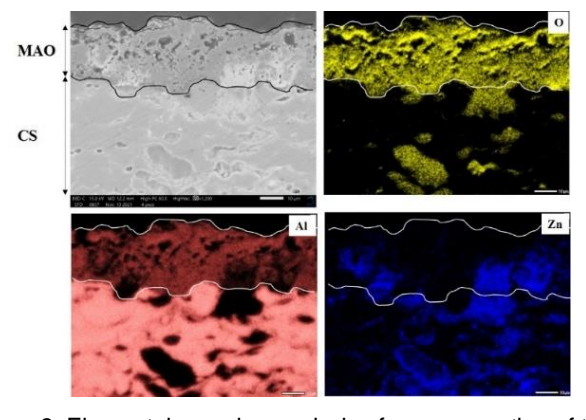


Figure 3. Elemental mapping analysis of a cross-section of the CS-MAO-30Zn sample.

Şekil 3. CS-MAO-30Zn numunesinin kesit yüzeyinin elementel haritalama analizi.



#### 3.2 Wear tests

Figure 4 presents the friction curves of MAO and CS-MAO-Zn samples under testing loads of 1–4 N for a total sliding distance of 50 m. Under 1 N load, all CS-MAO-Zn samples exhibited a lower coefficient of friction (COF) than the MAO sample, indicating that the preliminary CS process before MAO significantly enhanced tribological properties. Specifically, the CS-MAO-30Zn sample consistently demonstrated a lower COF across all testing loads. Additionally, the friction curve of the CS-MAO-30Zn sample exhibited the smoothest trend for all loads, whereas the other samples displayed slight fluctuations or an increasing COF pattern. According to these findings, Zn-enriched CS layers reduced friction and improved coating stability during dry sliding at RT.

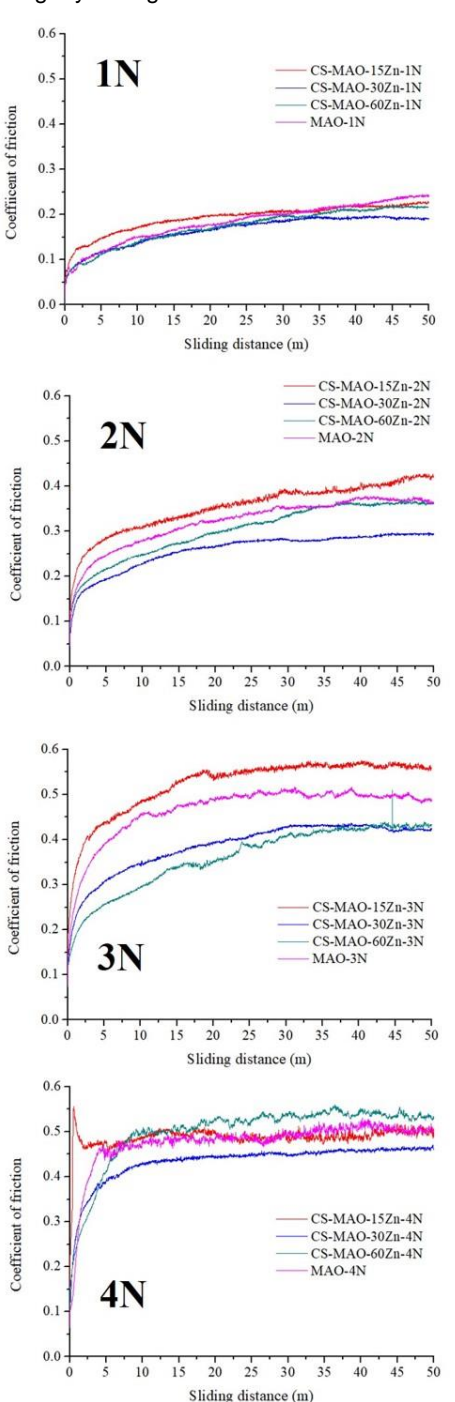


Figure 4. Friction curves of the MAO and CS-MAO-Zn samples for each load.

Şekil 4. Her yük için MAO ve CS-MAO-Zn numunelerinin sürtünme eğrileri.

Figure 5 presents the steady-state COF values of MAO and CS-MAO-Zn samples under different testing loads. The COF values increased with rising loads up to 3 N for all coatings, except for the CS-MAO-15Zn sample, which exhibited a lower COF at 4 N than at 3 N. Under 1 N load, all CS-MAO-Zn samples had a lower COF than the MAO sample, confirming that the preliminary CS process significantly improved tribological performance. The CS-MAO-30Zn sample consistently exhibited the lowest COF across all testing loads, with values of 0.18, 0.28, 0.42, and 0.45 for 1, 2, 3, and 4 N loads, respectively. It was found that MAO coatings on 30 wt.% Zn-containing CS'ed samples provided the most favourable conditions for reducing steady-state COF.

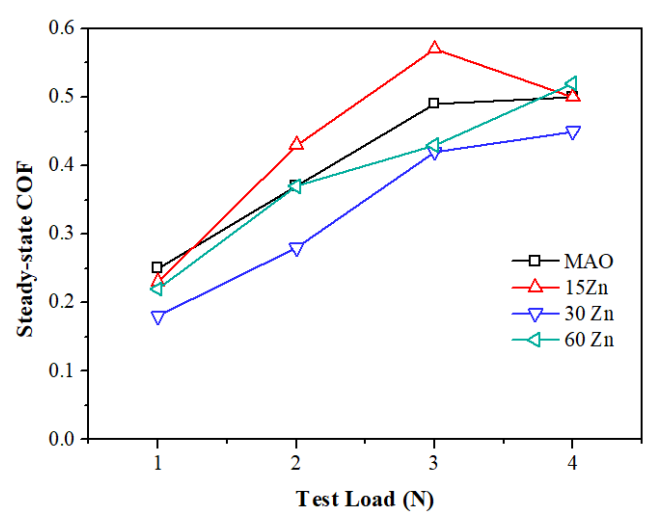


Figure 5. Steady-state COF values of MAO and CS-MAO-Zn samples.

Şekil 5. MAO ve CS-MAO-Zn numunelerinin kararlı durum sürtünme katsayısı değerleri.

Figure 6a presents the volumetric wear loss per sliding distance for MAO and CS-MAO-Zn samples under different testing loads. Across all loads, CS-MAO-Zn samples exhibited lower wear loss compared to the MAO sample, demonstrating the effectiveness of Zn-enriched CS layers in enhancing wear resistance. A significant increase in wear loss was observed at 4 N, whereas the wear rate remained relatively stable under 3 N load conditions. This suggests a notable shift in the wear mechanism at 4 N, which is transitioning from mild to severe wear. Figure 6b provides linear fitting lines for volumetric loss/sliding distance values with standard deviations for 1 N, 2 N, and 3 N loads as well as coefficient of determination (R²) values. It should be noted that the wear rate of the CS-MAO-30Zn sample was five times lower than that of the MAO sample, demonstrating improved wear resistance.

These results revealed that CS-MAO-30Zn and CS-MAO-60Zn samples exhibited similar wear loss trends, confirming their enhanced wear resistance. The MAO coatings applied to CS'ed samples demonstrated significantly improved wear performance compared to those fabricated directly on the substrate. Further, in order to evaluate the accuracy of the linear fitting lines, R² values were calculated, as shown in Figure 6b, which provided a quantitative measure of the quality of the fitted models.



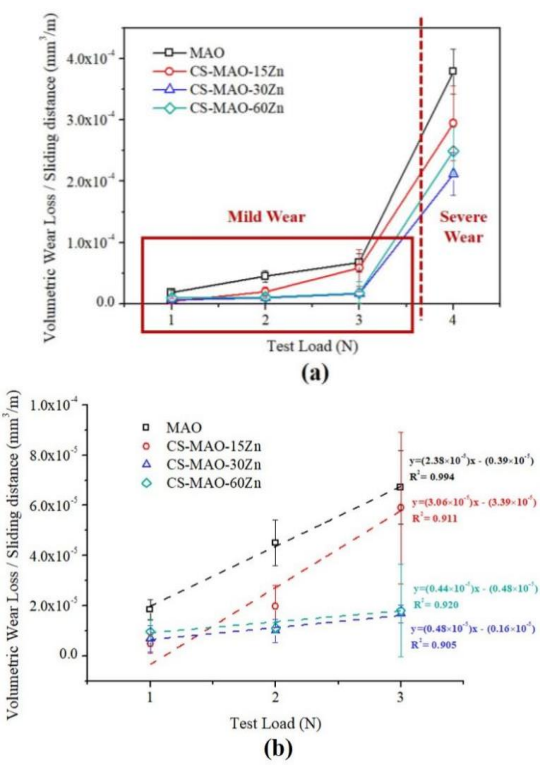


Figure 6. (a) Volumetric wear loss/sliding distance values of MAO and CS-MAO-Zn samples for each test load and (b) linear fitting lines for volumetric loss/sliding distance values with the coefficient of determination (R²) values. Şekil 6. (a) Her yük için MAO ve CS-MAO-Zn numunelerinin hacimsel aşınma kaybı/kayma mesafesi değerleri, (b) hacimsel aşınma kaybı/kayma mesafesi değerleri için doğrusal uyum çizgileri ve belirleme katsayısı (R²) değerleri.

Figure 7 presents the surface SEM images of wear tracks formed under 2 N and 4 N loads for a sliding distance of 50 m. Under 2 N load, slight spallation regions were observed in all MAO and CS-MAO-Zn samples, with small cracks appearing on the wear track surfaces of MAO and CS-MAO-15Zn samples. When the load increased to 4 N, the spallation regions became more apparent, indicating more intensive wear. Additionally, deep cracks were observed on the wear track surfaces of all MAO and CS-MAO-Zn samples, except for the CS-MAO-30Zn sample, which exhibited a more uniform and crack-resistant wear surface.

Figure 8 presents surface SEM images of these wear tracks after the 50 m sliding distance wear test. In order to determine the wear mechanism, wear tracks formed on MAO and CS-MAO-Zn samples under a 3 N load were examined using SEM at low (X200) and high (X2000) magnifications. The wear tracks, outlined by red dashed lines in X200 magnification images (left side), were clearly visible. The CS-MAO-30Zn sample exhibited the smallest wear track area, significantly smaller than those of the CS-MAO-15Zn, CS-MAO-60Zn, and MAO samples. Under 3 N load conditions, the wear track on the CS-MAO-30Zn sample was very small, therefore, it was hardly detectable.

At high magnification, spallation regions (marked with red circles) were observed in the SEM images of all wear tracks. However, the CS-MAO-30Zn sample exhibited fewer spallation regions than the others. Additionally, deep cracks (indicated by red arrows) without a network structure were visible in the wear tracks of CS-MAO-15Zn and CS-MAO-60Zn samples. These findings confirmed that CS-MAO-30Zn demonstrated the best tribological properties, outperforming both the MAO and other CS-MAO-Zn samples. Moreover, while increasing Zn content to 60 wt.% led to significant coating deterioration, a 15 wt.% Zn content was insufficient to enhance wear resistance effectively.

These observations were further supported by wear track examinations conducted under a 3 N load, where higher porosity and deep cracks were evident in coatings with excessive Zn content.

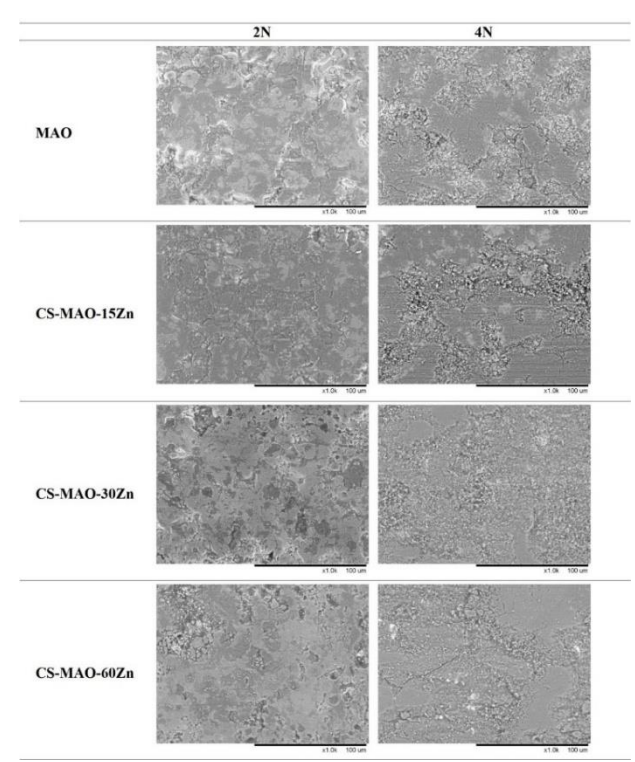


Figure 7. Surface SEM images of wear tracks formed under the load of 2 N and 4 N for MAO and CS-MAO-Zn samples. Şekil 7. MAO ve CS-MAO-Zn numunelerinde 2 N ve 4 N yük altında oluşan aşınma izlerinin yüzey SEM görüntüleri.

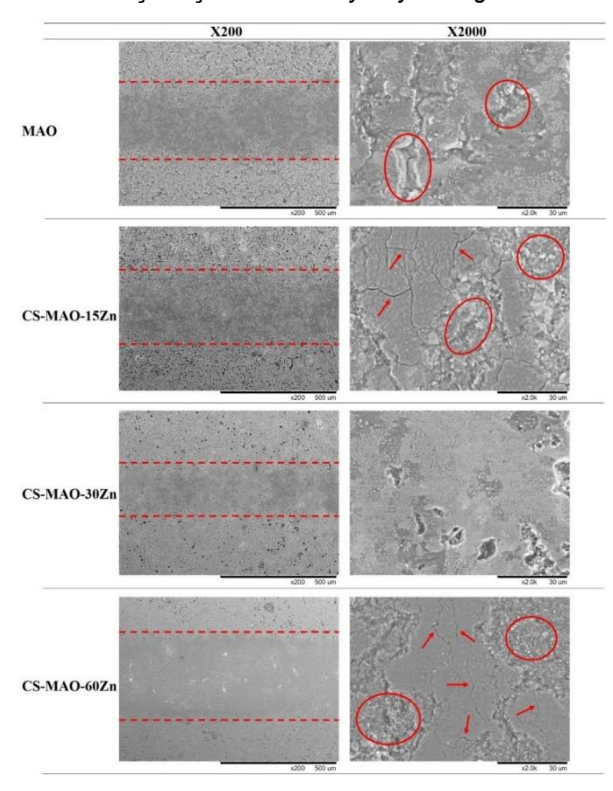


Figure 8. Surface SEM images of wear tracks formed under the load of 3 N for MAO and CS-MAO-Zn coatings with low and high magnifications.

Şekil 8. MAO ve CS-MAO-Zn kaplamalarda 3 N yük altında oluşan aşınma izlerinin düşük ve yüksek büyütmeli yüzey SEM görüntüleri.

Kullu et. al. ITU 2025



#### 4. Discussion

The present study investigated the tribological performance of Zn-enriched CS layers followed by MAO coatings on 7075 Al alloy. The results demonstrated that the incorporation of Zn in the CS layers significantly influenced the frictional and wear behaviour of the MAO coatings. It was observed that the CS layer significantly contributed to the reduction of COF values in all Zn-containing coatings compared to the conventionally MAO-coated 7075 Al alloy. The friction curves revealed that CS-MAO-Zn samples, specifically CS-MAO-30Zn, exhibited smoother frictional characteristics that indicated a stable sliding interaction with the Al<sub>2</sub>O<sub>3</sub> counterface. improvement is primarily attributed to the presence of Zn/ZnO phases, which acted as lubricating agents in the coating. The formation of ZnO during the MAO process was evident from XRD analysis, supporting Zn-enriched coatings facilitated a self-lubricating effect (Cetiner, Atar, Derin, & Cimenoglu, 2020). Prior studies have shown that ZnO possesses a wurtzite structure and can form a lubricating tribolayer, therefore, it can enhance the tribological performance of ceramic-based coatings under dry sliding conditions (Mohedano & Arrabal, 2021).

In terms of wear resistance, volumetric wear loss measurements demonstrated that Zn-enriched CS layers substantially improved the durability of MAO coatings. The wear rate of CS-MAO-30Zn was found to be approximately five times lower than that of the conventional MAO coating. The SEM analysis of worn surfaces further supported these findings, showing fewer spallation regions and microcracks on the CS-MAO-30Zn sample. The influence of Zn content on coating microstructure was also evident from cross-sectional SEM images. The CS-MAO-30Zn sample exhibited a relatively uniform and compact microstructure, with fewer large pores compared to CS-MAO-60Zn. Since CS-MAO-60Zn contains a high amount of Zn, it negatively affected the mechanical strength and wear resistance of the coating, which can be due to high porosity and reduced electrical conductivity of the CS layer.

The wear mechanisms observed in this study were predominantly characterised by mild wear for CS-MAO-30Zn, whereas higher wear rates were obtained from MAO and CS-MAO-60Zn samples. It is suggested that the presence of Zn/ZnO in the CS-MAO-30Zn coating provided a protective layer on the wear track for reducing direct contact with the counterface. In contrast, the higher porosity containing MAO coating of the CS-MAO-60Zn sample generated higher wear debris accumulation, leading to more severe material removal and surface damage.

#### 5. Conclusion

In the present study, MAO coatings on Zn-enriched CS layers on 7075 Al alloy were investigated to determine their microstructural characteristics and tribological performance under dry sliding contact at RT. The key findings are outlined below.

- The MAO, CS-MAO-15Zn, and CS-MAO-30Zn samples had a uniform external coating with a thickness of ~25 μm, while CS-MAO-60Zn had a non-uniform and thinner external coating (~15 μm). CS-MAO-30Zn had the lowest surface roughness (0.84 μm), while the MAO sample exhibited the highest roughness (1.56 μm). Porosity was highest in CS-MAO-60Zn, whereas CS-MAO-30Zn had small, evenly distributed pores.
- The CS-MAO-30Zn sample exhibited the lowest COF and smoothest friction curve, attributed to the lubricating effect of ZnO. Although the presence of ZnO improved the wear resistance, excess Zn (60 wt.%) led to the generation of

defective MAO coating. 15 wt.% Zn in the CS layer was insufficient to enhance tribological properties compared to MAO coating fabricated on 7075 Al alloy. However, the CS layer containing 30 wt.% Zn provided the lowest COF and wear resistance after the MAO process.

 As the test load increased for MAO and CS-MAO-Zn coatings, a transition from mild wear to severe wear was observed at the 3 N threshold load.

Lightweight aluminium components exposed to severe operating conditions can benefit from this coating approach, which is particularly beneficial for the aerospace, automotive, and marine industries.

#### 6. Acknowledgements

The authors are grateful for the financial support from Istanbul Technical University Scientific Research Projects (ITU-BAP, Project Number: 43157). The submitted article titled "Enhanced Tribological Performance of Micro-Arc Oxidation Coatings on 7075 Aluminium Alloy via Zn-Enriched Cold Spray Layers" was prepared by the M.Sc. thesis of Ms. G. Kullu.

#### 6. Conflicts of Interest

The authors declare no conflict of interest.

#### 7. References

- Cetiner, D., Atar, E., Derin, B., & Cimenoglu, H. (2020). Thermal oxidation of cold sprayed Ti-5Al-XZn coatings for tribological applications. *Materials Letters*, 274, 127959. Retrieved from https://doi.org/10.1016/j.matlet.2020.127959
- Curran, J. A., & Člyne, T. W. (2006). Porosity in plasma electrolytic oxide coatings. *Acta Materialia*, 54(7), 1985– 1993. Retrieved from https://doi.org/10.1016/j.actamat.2005.12.029
- Gándara, M. J. F. (2013). Aluminium: The metal of choice. *Materiali in Tehnologije*, 47(3), 261–265. Jiang, B. L., & Wang, Y. M. (2010). Plasma electrolytic
- Jiang, B. L., & Wang, Y. M. (2010). Plasma electrolytic oxidation treatment of aluminium and titanium alloys. In Woodhead Publishing Series in Metals and Surface Engineering (pp. 110–154). Cambridge: Woodhead Publishing Limited. Retrieved from https://doi.org/http://dx.doi.org/10.1533/978184569945 1.2.110
- Kaba, M., Muhaffel, F., Malayoglu, U., & Cimenoglu, H. (2024). Surface modification of WE43 Mg alloy via combination of cold spray and micro-arc oxidation for wear related applications at high temperatures. Surface and Coatings Technology, 494(P3), 131530. Retrieved from https://doi.org/10.1016/j.surfcoat.2024.131530
- Lu, X., Mohedano, M., Blawert, C., Matykina, E., Arrabal, R., Kainer, K. U., & Zheludkevich, M. L. (2016). Plasma electrolytic oxidation coatings with particle additions – A review. Surface and Coatings Technology, 307, 1165– 1182. Retrieved from https://doi.org/10.1016/j.surfcoat.2016.08.055
- Lv, X., Cao, L., Wan, Y., & Xu, T. (2019). Effect of different electrolytes in micro-arc oxidation on corrosion and tribological performance of 7075 aluminum alloy. *Materials Research Express*, 6(8). Retrieved from https://doi.org/10.1088/2053-1591/ab1da5
- Mohedano, M., & Arrabal, R. (2021). Plasma Electrolytic Oxidation (PEO) Coatings. In *Plasma Electrolytic Oxidation (PEO) Coatings* (p. 238). MDPI. Retrieved from https://doi.org/10.3390/books978-3-0365-0553-4



- Muhaffel, F., Baydogan, M., & Cimenoglu, H. (2021). A study to enhance the mechanical durability of the MAO coating fabricated on the 7075 Al alloy for wear-related high temperature applications. *Surface and Coatings Technology*, 409(October 2020), 126843. Retrieved from https://doi.org/10.1016/j.surfcoat.2021.126843
- Prasad, N. E., & Wanhill, R. J. H. (2016). *Aerospace Materials and Material Technology* (Vol. 1). Singapore: Springer.
- Rama Krishna, L., Somaraju, K. R., & Sundararajan, G. (2003). The tribological performance of ultra-hard ceramic composite coatings obtained through microarc oxidation. Surface and Coatings Technology, 163, 484–490. Retrieved from https://doi.org/10.1016/S0257-8972(02)00646-1
- Tazegul, O., Muhaffel, F., Meydanoglu, O., Baydogan, M., Kayali, E. S. S., & Cimenoglu, H. (2014). Wear and corrosion characteristics of novel alumina coatings produced by micro arc oxidation on AZ91D magnesium alloy. Surface and Coatings Technology, 258, 168–173. Retrieved from https://doi.org/10.1016/j.surfcoat.2014.09.035
- Yang, X., Chen, L., Jin, X., Du, J., & Xue, W. (2019). Influence of temperature on tribological properties of microarc oxidation coating on 7075 aluminium alloy at 25 °C 300 °C. *Ceramics International*, 45(9), 12312–12318. Retrieved from https://doi.org/10.1016/j.ceramint.2019.03.146

Kullu et. al. ITU 2025